J Mater Sci (2011) 46:6390–6395
DOI 10.1007/s10853-011-5587-4

Influence of ion energy on damage induced by Au-ion implantation in silicon carbide single crystals

Aurélie Gentils · Florence Linez · Aurélien Canizarès · Patrick Simon · Lionel Thomé · Marie-France Barthe

Received: 23 November 2010 / Accepted: 25 April 2011 / Published online: 7 May 2011
© Springer Science+Business Media, LLC 2011

Abstract This article reports on the influence of the ion energy on the damage induced by Au-ion implantation in silicon carbide single crystals. 6H-SiC samples were implanted with Au ions at room temperature at two different energies: 4 and 20 MeV. Both Rutherford Backscattering spectrometry in channelling geometry (RBS/C) and Raman spectroscopy were used to probe the ion implantation-induced damage. Results show that the accumulated damage increases with the fluence up to the amorphization state. RBS/C data indicate that 4-MeV implantation induces more damage than 20-MeV implantation at a given fluence. This effect is attributed to nuclear collisions since the amount of damage is identical at 4 or 20 MeV when the fluence is rescaled in dpa. Surprisingly, Raman data detect more damage for 20-MeV implantation than for 4-MeV implantation at low fluence (below 10^{13} cm^{-2}) where point defects are likely formed.

Introduction

When materials are submitted to radiation with energetic particles such as ions, their atomistic structures are altered: atoms may switch positions with each other, or even be removed from their lattice sites. The accumulation of these defects leads to damage of the material. It is, therefore, important to understand the response of materials under radiation environments in order to predict their performance for nuclear applications. Silicon carbide (SiC) has been proposed for use in the future high temperature gas cooled nuclear reactors either as a cladding material for the nuclear fuel or as a structural material for the reactor core. Due to the early interest for the development of the ion implantation doping process in SiC, previous studies were mainly focused on low energy ion implantation (~100 keV) [1, 2]. Some of them were focused on the effect of fluence, ion flux or/and temperature [3, 4], others on damage induced by ion implantation and diffusion of the implanted species [5]. But none of them studied the effect of the ion energy on the induced damage in silicon carbide.

In this study, the combination of Rutherford Backscattering Spectrometry in channelling mode (RBS/C) and Raman spectrometry is used in order to study the effect of the ion energy on the created damage in silicon carbide single crystals.

A. Gentils · F. Linez · A. Canizarès · P. Simon · M.-F. Barthe
CNRS, UPR 3079, CEMHTI, 45071 Orléans, France

A. Gentils · F. Linez · A. Canizarès · P. Simon · M.-F. Barthe
Université d'Orléans, 45067 Orléans Cedex 2, France

A. Gentils (✉) · L. Thomé
CSNSM, CNRS/IN2P3, Univ Paris-Sud, Bât. 108,
91405 Orsay Cedex, France
e-mail: Aurelie.Gentils@csnsm.in2p3.fr

Experimental

Single crystalline n-type 6H-SiC specimens obtained from CREE, Inc., were used in this study. The surface was normal to the [0001] crystallographic axis, and polished to an optical finish grade. The specimens were implanted at room temperature with 4 MeV Au^{2+} and 20 MeV Au^{6+} ions using ion accelerators of CSNSM, Orsay (France) and of Instituto de Fisica, Universidade Federal do Rio Grande do Sul, Porto Alegre (Brazil), respectively. The ion fluence was varied in the range 10^{12}–10^{15} cm^{-2}, and the substrates were tilted ~7° from the direction of the incident ion beam

in order to reduce ion-channelling effects. In both cases, the ion flux was sufficiently low to avoid target heating during irradiation: at Porto Alegre, it was 1.6×10^{11} ion cm^{-2} s^{-1}, and at Orsay it was 1.3×10^{12} ion cm^{-2} s^{-1}. Taking into account the energy deposition for 20- and 4-MeV particles, the dissipated power in the material per ion and per surface is of the same order (3.2×10^{12} MeV ion cm^{-2} s^{-1} for 20-MeV ions, and 6.5×10^{12} MeV ion cm^{-2} s^{-1} for 4-MeV ions), so a comparison between each set of irradiation is possible at a given fluence.

According to SRIM Monte Carlo calculations [6], which do not take into account defect recombinations, the damage corresponding to a fluence of 10^{15} cm^{-2} was 5.2 dpa (displacement per target atom, for both Si and C atoms) at the peak maximum of the damage profile for 4-MeV Au ions and 3.2 dpa for 20-MeV Au ions. The projected ion range (R_p) was equal to 0.5 µm for the 4-MeV ions and 3 µm for the 20-MeV ones. The nuclear and electronic stopping powers, respectively, S_n and S_e, calculated from SRIM software are plotted in Fig. 1 as a function of the depth into the material for 4 and 20 MeV Au ions. The displacement energies used in these calculations were 19 eV for the Si sublattice and 20 eV for the C one [7].

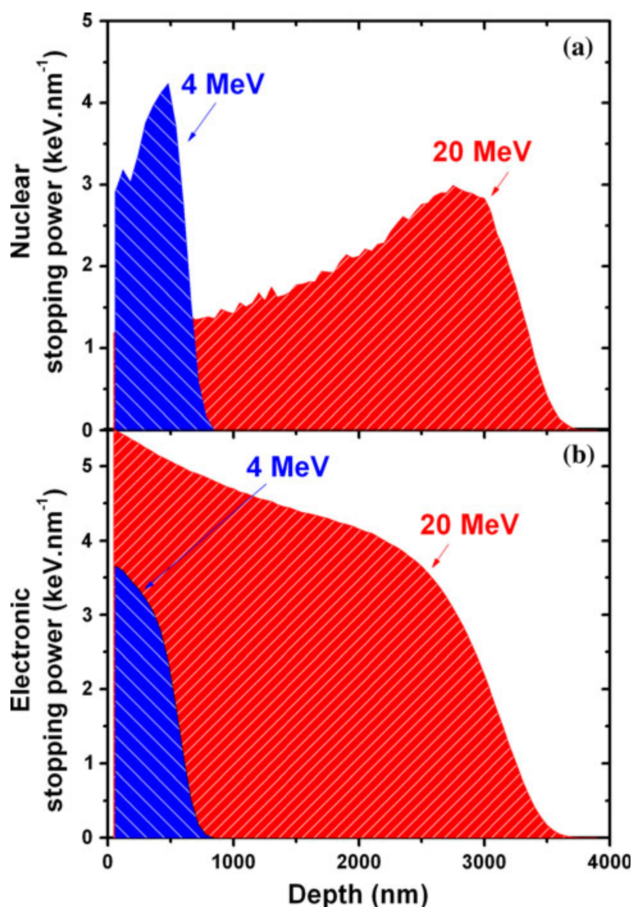

Fig. 1 Nuclear (**a**) and electronic (**b**) stopping powers calculated from SRIM versus depth for 4 and 20 MeV Au ion implanted silicon carbide single crystals

RBS/C spectra were recorded in random and aligned geometry using the ARAMIS ion accelerator at the CSNSM, Orsay. A 1.4 MeV He^+ beam was used for the characterization of the radiation damage at room temperature. Monte Carlo simulations of RBS/C spectra were performed using the McChasy code in order to quantify the fraction of disorder as a function of depth in the crystal [8]. The probed region by RBS/C was around 1 µm.

Raman spectra were recorded with a Renishaw Invia Reflex spectrometer coupled with a Leica DM2500 microscope, with a $\times 100$ objective, in confocal mode. The spectrometer acts in single spectrometer configuration with an Edge filter (with low-frequency cutoff at around 150 cm^{-1}) and a 2400 g mm^{-1} grating. The excitation line was the 457 nm line of an Ar^+ laser, with power on the sample of the order of 1 mW. The laser beam is focused on the sample surface rather than some micrometers below, in order to have reliable data on the whole set of samples, which present very different absorption coefficients in the visible range due to the different degrees of damage. The confocal filtering limits the probed thickness to about 1 µm, this thickness is even more decreased down to some hundreds of nanometers for the most damaged samples close to the surface.

It is worth noting that the probed area (up to 1 µm, whatever RBS/C or Raman is used) includes all the cascades occurring for 4 MeV Au ions, while it corresponds only to the beginning of the slowing down of 20 MeV Au ions in 6H-SiC single crystals.

Results and discussion

A set of typical RBS/C spectra obtained from samples implanted with 4 and 20 MeV Au ions at indicated fluences are presented in Fig. 2. A spectrum of a randomly oriented virgin sample rotating around the [0001] axis as well as a channelled spectrum along the same sample axis are also shown. The spectrum taken in a random direction displays two plateaus below 800 and 350 keV that correspond to the backscattering of analyzing particles from the Si and C atoms of the sample, respectively. The spectrum taken in the ⟨0001⟩-axial direction on the virgin crystal displays the same features with a much lower backscattering yield in both Si and C regions due to the channelling effect. The ratio of channelled to random spectra near the surface was about 3%, thus showing the good single crystalline quality of the material. For each implanted sample, this ratio increased with the fluence, indicating the presence of point defects (as evidenced by positron annihilation spectroscopy

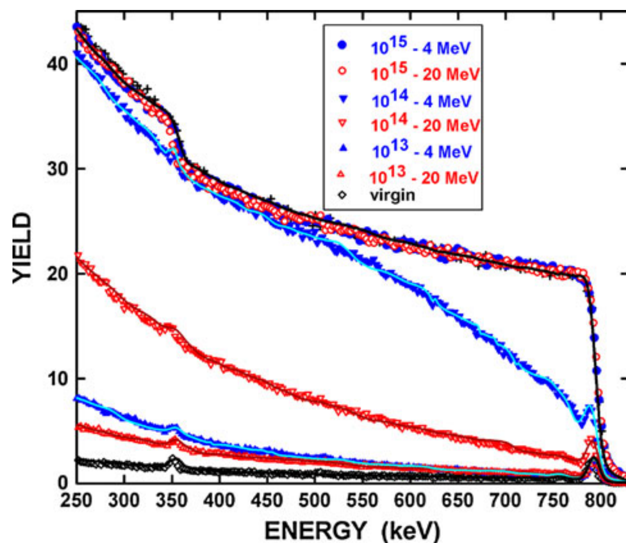

Fig. 2 RBS/C spectra channelled in the [0001] direction from virgin crystal and samples implanted with 4 or 20 MeV Au ions at indicated fluences. A random spectrum of a rotating virgin sample is also included. *Lines* are fits to RBS/C data with the McChasy Monte Carlo code [8]

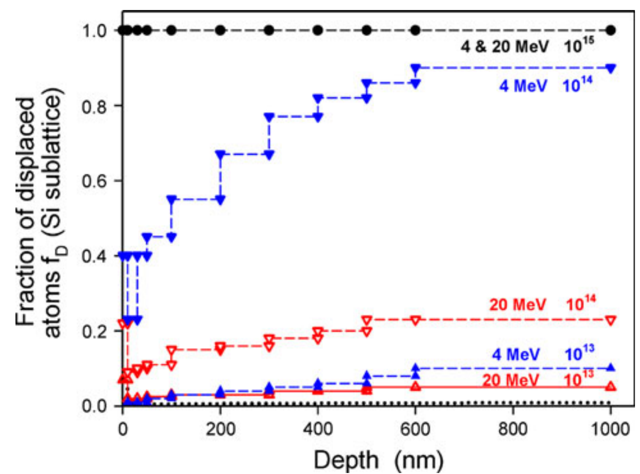

Fig. 3 Fraction of displaced atoms (f_D) corresponding to the Si lattice as a function of depth into the sample, extracted from McChasy Monte Carlo simulations

in [9]), that can cause direct backscattering of channelled ions and dechannelling. At 10^{13} cm^{-2}, the aligned spectra recorded on 4-MeV implanted samples show a highest yield than the 20-MeV ones, meaning that the material is more damaged. The same effect occurs also at a fluence of 10^{14} cm^{-2}, and it is more pronounced. At 10^{15} cm^{-2}, the recorded spectra correspond to the random spectra whatever is the ion energy, showing that the fraction of displaced silicon atoms is at its maximum. It indicates that in this case the material is totally disordered. Lines represent fits to the RBS/C spectra using McChasy Monte Carlo simulation code [8]. Calculations rely on the basic assumption that Si and C atoms are randomly displaced from their original lattice sites during ion implantation. From these simulations the fraction of displaced atoms (f_D) corresponding to the Si lattice was extracted as a function of depth into the sample (Fig. 3). The variation of accumulated damage taken at the depth for which this measured fraction of displaced atoms is maximum (f_D^{max}) (i.e., between 0.8 and 1 µm for both 4 and 20 MeV ions as seen in Fig. 3) is shown as a function of the Au ion fluence in Fig. 4a. Solid lines are fits to the experimental data with the MSDA model [10, 11] using $n = 1$ (one step of damage accumulation). The accumulated damage in the Si lattice is close to zero at 10^{12} cm^{-2} for both ion energies. It increases as a function of the ion fluence up to a plateau at a value of 1, corresponding to the total disorder for both 4- and 20-MeV. It is worth noting that above 10^{12} cm^{-2}, the accumulated damage is, at a given ion fluence, always higher at 4 MeV than at 20 MeV. This will be discussed below.

Raman spectra of virgin and implanted SiC are shown in Fig. 5 where the Raman intensity is plotted versus the wavenumber shift with respect to the laser. Samples implanted at 4 MeV are represented on the left part, and those implanted at 20 MeV are on the right part. For virgin samples, three main sharp lines are observed at 767, 790, and 964 cm^{-1}, with less intense lines lying at 140 and 797 cm^{-1}. These lines correspond to the expected spectrum of 6H-SiC, as firstly reported by Feldman et al. [12]. These sharp lines are also observed for samples implanted at low fluence (10^{12} cm^{-2}). The lower intensity of more implanted samples denotes a growing damage upon increasing fluence. A clear progressive crossover appears, from crystalline (sharp symmetric lines) to amorphous (broader envelope due to phonon density of states, Raman-allowed by the symmetry lowering induced by damaging). This amorphization of SiC under irradiation was already reported for various conditions of irradiation [13–16]. It is visible at the lowest fluence (10^{12} cm^{-2}) for 20 MeV, where a broad background becomes visible, nothing detectable is observed on the corresponding 4 MeV data, apart from a small intensity loss for the 964 cm^{-1} line. For 20 MeV, the main sharp lines appear also slightly broadened. The 10^{13} cm^{-2} data (4 and 20 MeV) show coexistence of the crystalline peaks and of the density of states, the latter being dominant in the 20 MeV sample. For higher fluences (10^{14} and 10^{15} cm^{-2}), only the density of states is observed for both ion energies. For each of these two fluences, the broad features on this density of states appear somewhat more resolved for 20 MeV sample than for the 4 MeV one. It is particularly clear on the 10^{14} cm^{-2} data, where the change of slope characteristic of the end of the 1st order density of states, near 970 cm^{-1}, is more resolved on 20 MeV sample compared to 4 MeV one. Then the disorder

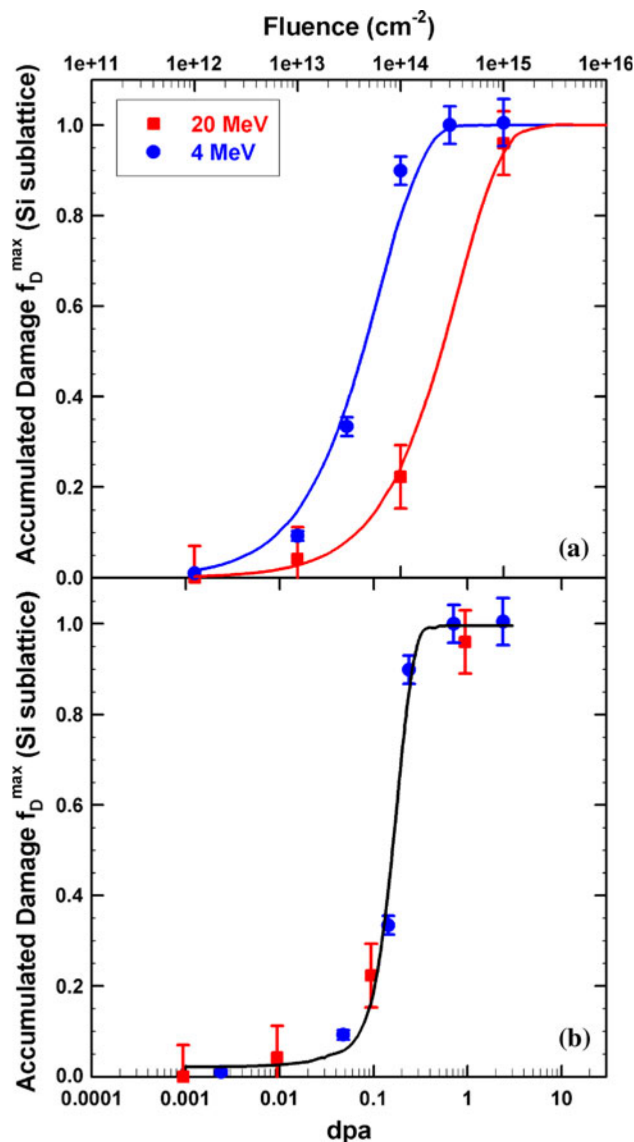

Fig. 4 Accumulated damage (f_D^{max}) in the Si sublattice for 4 MeV (*circle*) and 20 MeV (*square*) implanted 6H-SiC single crystals versus **a** fluence; **b** dpa calculated using SRIM [6] as the integral of the area under the curve between 0 and 1 μm. *Solid lines* are fits to the experimental data with the MSDA model using $n = 1$ [10, 11]

probed by Raman at 4 MeV looks more important than at 20 MeV for the two highest fluences. To summarize, the 20 MeV sample look to be more damaged than the 4 MeV one up to 10^{13} cm^{-2}, above this fluence it is the contrary.

The sensitivity of RBS/C and Raman techniques for the atomic rearrangements occurring at low and high fluences is different. RBS/C essentially detects atomic displacements. Raman spectroscopy may also detect defects inducing a release of the Brillouin zone-center selection rules: this includes creation of point defects such as colored centers and other electronic-like defects, even present at low concentration. However, the change of the Raman response due to atomic displacements is stronger than that induced by points defects invoked previously: the selection rules are released in both cases, but atomic displacements imply a supplementary disorder in the phonon density of states. These features explain the more disordered-like density of states obtained for the 4 MeV samples as compared to the 20 MeV ones at the two highest fluences. They can also explain the appearance of a small background and the beginning of line broadening observed for the 20 MeV sample at 10^{12} cm^{-2} (Fig. 6).

At low fluences (i.e., before amorphization), positron annihilation spectroscopy measurements show that different kinds of defects are created in both 4- and 20-MeV implanted crystals [17]. The formation of small interstitial-type defect(s) (clusters), which induce the development of a tensile elastic strain, was also observed by X-ray diffraction experiments in the low fluence range [18]. These defects might be due either to an effect of electronic stopping power (higher at 20 MeV than at 4 MeV) or to different morphologies of defects cascades (i.e., damage cascades with different densities, different spatial extensions, or different types of defects and/or defect clusters created in each cascade).

At high fluence, only amorphous domains are observed, as shown by Raman results, in agreement with Debelle et al. [18] study. The total Si sublattice disorder observed with RBS/C experiments in SiC implanted with 4 and 20 MeV Au ions at high fluence corresponds thus to amorphous SiC, in the light of Raman measurements. Moreover, we observe a more pronounced disorder in the Si sublattice in SiC single crystals implanted with lower ion energy, i.e., 4 MeV. Indeed irradiation effects detected in the first micrometer depth depend strongly on the incident ions' energy, as they result mainly from elastic nuclear interactions at low energy and inelastic interactions at high energy. It has been shown previously that 6H-SiC single crystals implanted with 700 keV I ions ($S_{nmax} = 3.1$ keV nm^{-1}) were totally disordered above 10^{14} cm^{-2}, and that RBS/C spectra recorded after 827 MeV Pb ions irradiations ($S_{nmax} = 0.1$ keV nm^{-1}) do not exhibit any significant damage at the highest fluence reached (2×10^{13} cm^{-2}) [19]. In the first micron below the surface (i.e., the depth probed by RBS/C and Raman measurements), the value of the nuclear stopping power S_n at the maximum of the distribution is equal to 1.4 keV nm^{-1} for 20 MeV ions (Fig. 1a). Its value is nearly four times higher for 4 MeV ions ($S_n = 4.2$ keV nm^{-1}). This is in agreement with our RBS/C results: lower damage at higher ion energy (with a lower value of S_n) is thus due to nuclear collisions effects. The electronic stopping power (Fig. 1b) could, however, play a non-negligible role in the case of 20 MeV Au ions. To study its role, the accumulated damage in the Si sublattice has been plotted as a function of the number of

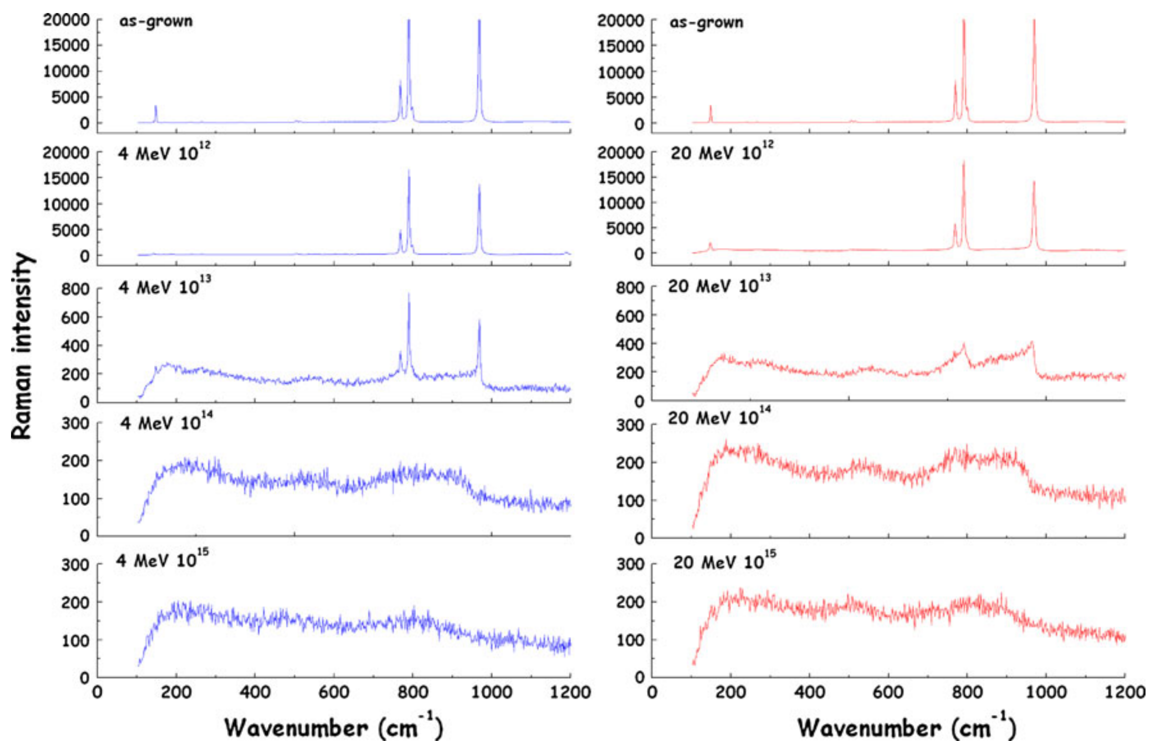

Fig. 5 Raman spectra of virgin 6H-SiC, 4-MeV implanted (*left column*) and 20-MeV implanted (*right column*) 6H-SiC single crystals, at indicated fluences

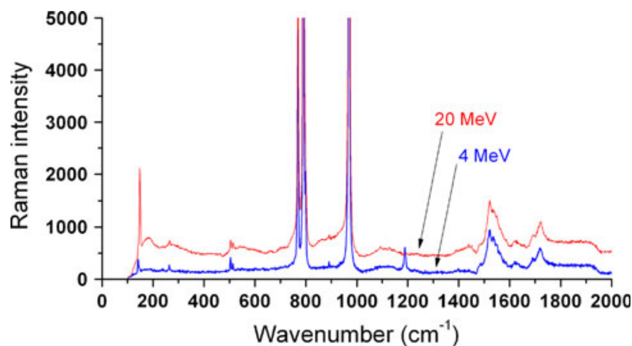

Fig. 6 Raman spectra of 6H-SiC crystals implanted at 10^{12} cm^{-2} with 4 and 20 MeV Au ions, respectively

displacement per atom (dpa), calculated by SRIM as an integral of the area under the curve between 0 and 1 µm (Fig. 4b). One can clearly see that the points are nicely superimposed: the accumulated damage is the same for 4 and 20 MeV at a given value of dpa. This result indicates that the electronic stopping power in the case of the 20 MeV ions do not lead to a partial annealing of defects induced by nuclear collisions. This is coherent with results obtained by Benyagoub et al. [19]. It has to be underlined that in the first micron depth, the electronic stopping power of 20 MeV Au ions ($S_e = 5.5$ keV nm^{-1}) is six times lower than for 827 MeV Pb ions ($S_e = 34$ keV nm^{-1}).

Conclusion

Damage in 6H-SiC single crystals after ion implantation at different energies has been followed by RBS/C and Raman spectroscopy. At low fluences Raman results show a beginning of disorder in the 20 MeV Au implanted crystals not observed in the 4 MeV ones, which could be attributed to point defects. This disorder could be induced by electronic slowing down, or due to different morphologies of defect cascades. At high fluence, Raman spectra show that the implanted materials become amorphous. The simulation of the RBS/C spectra by a Monte Carlo program (McChasy code) indicates that 4-MeV Au ion implantation induces more disorder in Si sublattice than 20-MeV one. This is attributed to the effect of nuclear collisions.

Acknowledgements The authors would like to thank the ARAMIS staff at CSNSM, Orsay, and Dr. Moni Behar, Porto Alegre, for their help with the ion implantations. This study was partially financed by the French "Groupement National de Recherche" (GNR) MATINEX, and by an ANR grant "RAMIRIS" no. 07-BLAN-0282-01.

References

1. McHargue CJ, Williams JM (1993) Nucl Instrum Methods Phys Res B 80:889
2. Brauer G, Anwand W, Coleman PG et al (1996) Phys Rev B 54:3084

3. Zhang Y, Weber WJ, Jiang W et al (2003) J Appl Phys 93:1954
4. Slotte J, Saarinen K, Janson MS et al (2005) J Appl Phys 97:033513
5. Audren A, Benyagoub A, Thome L et al (2007) Nucl Instrum Methods Phys Res B 257:227
6. Ziegler JF, Biersack JP, Littmark U (1985) In: The stopping and range of ions in solids. Pergamon, New York
7. Kerbiriou X, Barthe MF, Esnouf S, Desgardin P, Blondiaux G, Petite G (2007) J Nucl Mater 362:202
8. Nowicki L, Turos A, Ratajczak R, Stonert A, Garrido F (2005) Nucl Instrum Methods Phys Res B 240:277
9. Gentils A, Barthe MF, Egger W, Sperr P (2009) AIP Proc 1099:891
10. Jagielski J, Thomé L (2007) Vacuum 81:1352
11. Jagielski J, Thomé L (2009) Appl Phys A 97:147
12. Feldman DW, Parker JH Jr, Choyke WJ, Patrick L (1968) Phys Rev 170:698
13. Perez-Rodriguez A, Pacaud Y, Calvo-Barrio L, Serre C, Skorupa W, Morante JR (1996) J Electron Mater 25:541
14. Conrad J et al (1996) Nucl Instrum Methods Phys Res B 118:748
15. Bolse W (1998) Nucl Instrum Methods Phys Res B 141:133
16. Sorieul S, Costantini JM, Gosmain L, Thome L, Grob JJ (2006) J Phys Condens Mat 18:5235
17. Gentils A, Linez F, Barthe M-F (to be published)
18. Debelle A, Thomé L, Dompoint D, Boulle A, Garrido F, Jagielski J, Chaussende D (2010) J Phys D 43:455408
19. Benyagoub A, Audren A, Thomé L, Garrido F (2006) Appl Phys Lett 89:241914